Materials Science & Engineering A 564 (2013) 351–358

Contents lists available at SciVerse ScienceDirect

Materials Science & Engineering A

journal homepage: www.elsevier.com/locate/msea

Deformation mechanisms in a TiNi shape memory alloy during cyclic loading

Anne-Lise Gloanec [a,*], Giovambattista Bilotta [b], Michel Gerland [b]

[a] UME/MS–EnstaParistech–828 Boulevard des Maréchaux–91762 Palaiseau Cédex–France
[b] Institut P'–Département Physique et Mécanique des Matériaux–UPR3346–ENSMA–Téléport 2–1 Avenue Clément Ader, BP 40109, 86961 Futuroscope Chasseneuil Cédex–France

ARTICLE INFO

Article history:
Received 4 September 2012
Received in revised form
12 November 2012
Accepted 15 November 2012
Available online 27 November 2012

Keywords:
Low-Cycle Fatigue
Pseudoelastic Behaviour
Nanoindentation
Dislocations
Twinning
Shape Memory Alloy

ABSTRACT

The deformation mechanisms governing the cyclic stress-strain behaviour of a TiNi shape memory alloy were investigated in this work. To understand the development of these mechanisms during cyclic loading, three low-cycle fatigue tests were performed and stopped at different stages. The first test was stopped after the first cycle; the second one was stopped after 40 cycles, corresponding to the beginning of the stabilisation of the cyclic strain-stress behaviour; and the last one was carried out to failure (3324 cycles). Submitted to fatigue loading, the response of the TiNi shape memory alloy presents a classical pseudoelastic response. Two deformation mechanisms, identified by TEM observations, are highlighted, the first one by twins and the second by dislocation slip and its interaction with precipitates. These two mechanisms evolve without competition during cyclic loading. The nanomechanical properties of the alloy were also examined, and the evolution of the microhardness or indentation modulus was monitored.

1. Introduction

Shape memory alloys (SMAs) are widely applied in various industrial fields such as aeronautics, biomedicine, automotives and civil engineering and domestically [1,2]. TiNi alloys are popular SMAs due to their excellent biocompatibility and mechanical properties, including low weight, good corrosion resistance, and good fatigue strength [3,4]. SMAs are fascinating materials that exhibit properties not typically observed in ordinary metals and alloys. Indeed, TiNi shape memory alloys exhibit very specific thermomechanical behaviours, including a shape memory effect [3,5,6], good superelasticity [7–9] and a high damping capacity at room temperature [5,10,11]. Many engineering applications have been developed using some of these properties.

Within the frame of design and the reliability of systems using SMAs, it is essential to have phenomenological models that can predict the thermomechanical behaviour of these materials as close as possible to fatigue. Understanding the physical mechanisms governing the cyclic behaviour of SMAs and how they lead to degradation is a necessary step.

SMAs can undergo limited plastic deformation over a specific temperature range and then quickly revert back to their original shape in their high-temperature state through complete stress relaxation. Such behaviour is called superelasticity or pseudoelasticity. In this paper, we focus on this particular behaviour. The purpose of this study was to establish a relationship between cyclic loading and specific properties (transformation temperature, microhardness, indentation modulus), on the one hand, and deformation mechanisms, on the other hand.

2. Material and experimental test procedures

2.1. Material

A commercial TiNi shape memory alloy containing 51.3% (at.) Ti was used in this investigation. To develop pseudoelastic behaviour, a specific thermomechanical treatment was carried out. The various stages of this thermomechanical treatment have already been described elsewhere [12]. The resulting microstructure was mostly composed of fine grains with an average size of 25 μm.

2.2. Experimental test procedures

The test specimens used were cylindrical, with a gauge section measuring 8 mm in diameter, 20 mm in length and a total length of 120 mm. The gauge length was mechanically polished with silicon carbide paper to minimise the effects of surface irregularities, such as work hardening, due to machining or oxide layers developed at 850 °C, during the first step of the thermomechanical treatment. The surface was then finished by electrolytic polishing. Low-cycle fatigue (LCF) tests were conducted on a servo-hydraulic machine (MTS 810) controlled from 0 to 23 kN

* Corresponding author. Tel.: +33 169319750; fax: +33 169319906.
E-mail address: anne-lise.gloanec@ensta-paristech.fr (A.-L. Gloanec).

0921-5093/$ - see front matter © 2012 Elsevier B.V. All rights reserved.
http://dx.doi.org/10.1016/j.msea.2012.11.051

or 0 MPa to 485 MPa at 1 Hz. To induce the formation of the austenitic phase of the specimens, the tests were performed at 50 °C. This temperature was determined by differential scanning calorimetry. The signal was sinusoidal in shape with a null stress ratio. The strain amplitude was measured by an EPSILON extensometer with a root of 10 mm placed on the gauge of the test specimen. The objective of this work was to identify the deformation mechanisms that govern the cyclic-strain-stress (CSS) behaviour. Therefore, three LCF tests were performed and stopped at different stages. The first one was stopped after the first cycle; the second one was stopped after 40 cycles, corresponding to the beginning of CSS behaviour stabilisation [12–14]. The last test was performed until failure (N_f=3324 cycles).

After the fatigue tests, samples were cut from the gauge length of the test specimens for differential scanning calorimetry (DSC) measurements, for microhardness testing and for microstructural characterisation by transmission electron microscopy (TEM).

The first step in characterising a SMA material is to determine the characteristic transformation temperatures. There are several transformation temperatures, including the austenite start temperature (A_s) and the austenite finish temperature (A_f) during heating and the martensite start temperature (M_s) and the martensite finish temperature (M_f) during cooling. Additionally, an intermediate phase (R-phase) often appears during cooling, which exhibits its own start temperature (R_s) and finish temperature (R_f), before the transformation proceeds to martensite at lower temperature. All these transformation temperatures can be obtained by DSC measurements [15] with a TA DSC Q20 machine. Initially, the material specimen was cooled from approximately 80 °C to–50 °C and then heated from −50 °C to 80 °C. The starting and finishing temperatures of each transition phase (M_s, M_f, A_s, A_f, R_s and R_f), the peak temperatures (M_p, A_p and R_p) and the heat flow were determined from DSC thermograms. Note that several cycles of heating and cooling were carried out to ensure that there was no cycling effect on the transformation temperatures.

Microhardness tests were performed on samples polished to 1 μm with a Fischerscope H100C apparatus equipped with a square-base pyramidal indenter. Forty-nine square indentations (200 μm × 200 μm) were created in each sample with a load of 30 mN and a load application time of 15 s. A creep time of 15 s was also added at the maximum load before unloading. The microhardness, the indentation modulus and the creep behaviour were obtained for each sample.

The cyclic deformation microstructures were examined in a Phillips CM20 transmission electron microscope operated at 200 kV. Discs measuring 3 mm in diameter were cut from the gauge length of the bulk specimens near the fracture surface for samples tested until failure and from the middle of the gauge length for samples submitted to the two other tests. In each case, the discs were cut perpendicularly to the loading axis by electric-discharge machining. The thickness of the samples was reduced to about 75 μm by mechanical polishing. Electron-transparent foils for TEM were then prepared using the electrolytic double-jet technique with an electrolyte composed of 95% acetic acid and 5% perchloric acid. For each fatigue sample, several thin foils were studied to obtain large observation areas and to provide a representative point of view.

3. Results and Discussion

3.1. Cyclic strain-stress behaviour

The cyclic strain-stress behaviour of a TiNi shape memory alloy has already been presented elsewhere [7,12–14]. Tests were performed at 50 °C to induce the formation of the austenite phase. A classical pseudoelastic response was observed. An example of a characteristic loop is provided in Fig. 1. The hysteresis loop consists of six distinct segments. From O to A, the response corresponds to the elasticity of austenite. This linear curve is followed, from A to B, by a stress plateau where the transformation of austenite into martensite occurs continuously. At point B, the specimen is then completely in the martensite phase, and the response, from B to C, corresponds to the elasticity of this phase. Then, the stress is relaxed (point C). From C to D, the behaviour of the martensite phase is still elastic. The reverse transformation, from martensite to austenite, starts at point D and continues along the stress plateau, to point E. Finally, the material is completely in the austenite phase, and the response, from E to O, corresponds to the elasticity of austenite. In our case, at the end of the first cycle, no residual strain was observed. During cycling, the strain-stress response evolves and reaches a stabilised state. Indeed, the hysteresis loops are modified, changing their form and becoming smaller (Fig. 2). Nevertheless, this change tends to stabilise with the increasing number of cycles. This stabilisation effect typically occurs during the first 100 cycles [9]. In this study, stabilisation was reached in approximately 40 cycles.

Another way to present the cyclic behaviour is the dissipated energy versus the number of cycles [7,12], with the dissipated energy being equal to the surface of the hysteresis loop in the strain-stress curve. As reported in Fig. 2, the cyclic behaviour shows a rapid decrease during the first 50 cycles, followed by a slight decrease near the 500th cycle and then stabilisation until failure.

3.2. Differential Scanning Calorimetry

The transformation temperatures for each cycled sample were obtained from the DSC thermograms (heat flow vs. temperature, Fig. 3a for tested material and Fig. 3b for untested material).

To ensure that there was no cycling effect on the transformation temperatures, for each sample, two cycles of heating and cooling were performed. The heat flow curves, corresponding to both cycles on each sample, are quite similar, with very slight differences. When discernible, the peaks are always slightly higher in the second cycle.

It is well known that TiNi shape memory alloys exhibit two phases as a function of temperature: martensite and austenite [16–18]. Martensite transformations are solid-to-solid phase transformations that occur without diffusion or plasticity, potentially making them reversible. They involve changes in crystalline structure that can be induced by changes in either temperature or stress. The high-temperature, stress-free phase is called austenite (A-phase), which has a high-symmetry crystal structure typically

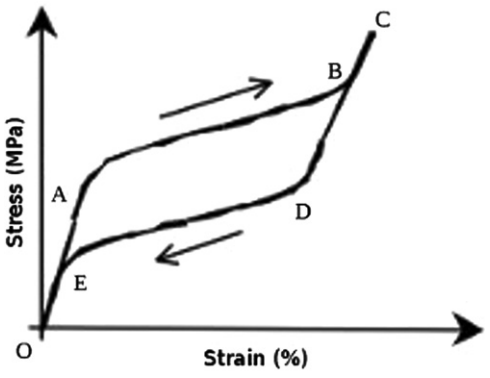

Fig. 1. An example of a pseudoelastic behaviour.

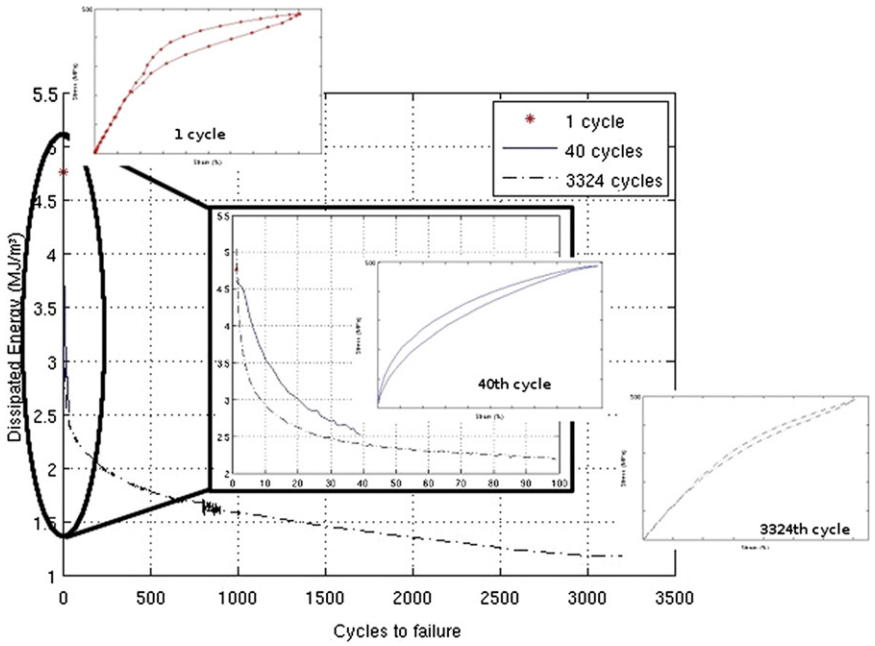

Fig. 2. Cyclic behaviour presented as dissipated energy versus number of cycles.

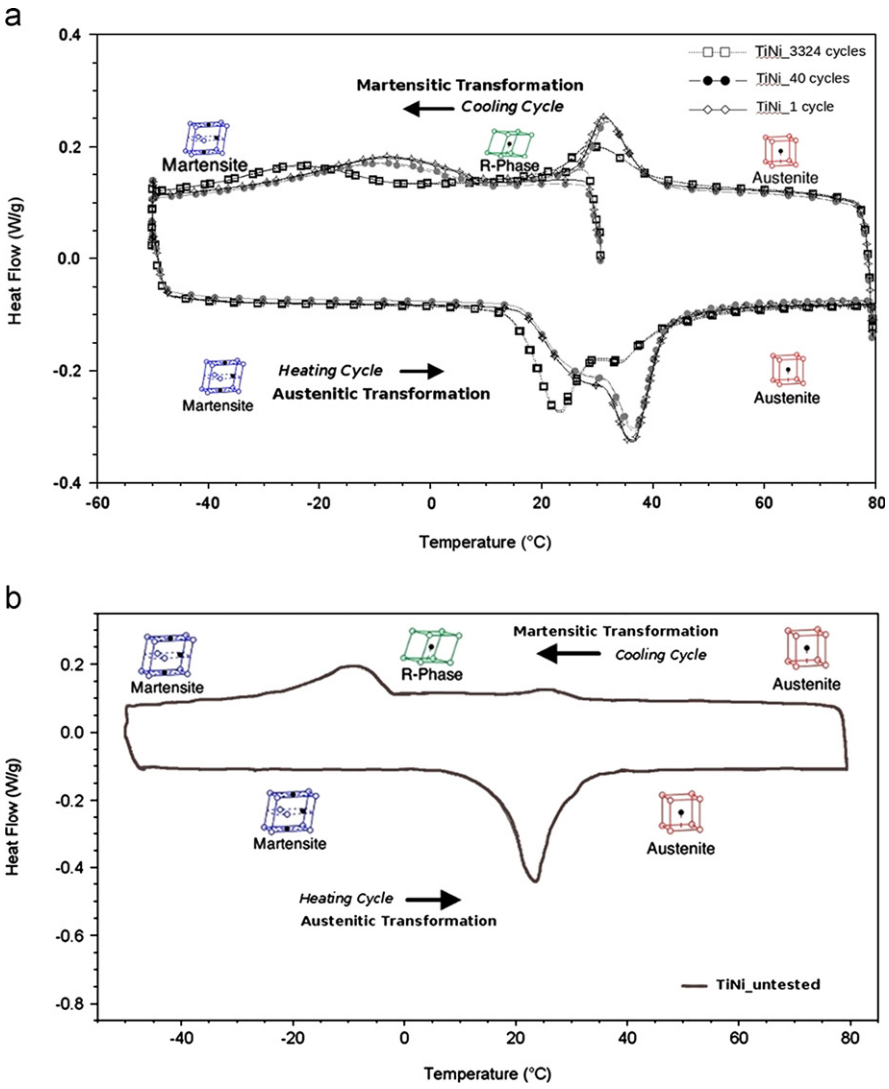

Fig. 3. a DSC ccurves for tested material (1 cycle, 40 cycles, 3324 cycles). b DSC curves for untested material.

based on a cubic lattice (CsCl structure or B2). The low-temperature, stress-free phase is called martensite (M-phase), which has a lower symmetry based on a monoclinic structure (B19′). In some special cases, there is an intermediate rhombohedral phase, a distortion of the B2 phase, known as the R-phase [6,10,17,19–23]. The formation of this phase is strongly influenced by the heat treatment of shape memory alloys [21,22,24]. As reported in Fig. 3b, for each sample, three heat flow peaks can be observed: a single stage M→A transformation during heating and two stages A→R→M transformation during cooling. The two samples, corresponding to the 1st cycle and to the 40th cycle, present the same behaviour during heating and during cooling, with slight differences. The curve corresponding to 40 cycles is slightly shifted to higher temperatures, and the peaks are slightly lower than those of the 1st cycle curve. As reported in Table 1, the transformation temperatures are roughly the same for each phase transformation. However, when the curves of the three samples are superimposed, marked differences are visible, mainly for the curve corresponding to 3324 cycles. For the peak corresponding to the martensite transformation, the shift toward lower temperature is quite substantial; however, this is not the case for the other peaks (Table 1). The heights of the peaks are similar between 1 cycle and 40 cycles but strongly decreases between 40 cycles and 3324 cycles. The areas of the peaks are quite similar for the two first curves (1 and 40 cycles) but much lower for the curve corresponding to 3324 cycles. Another difference is observed with the respect to the double peak of the austenitic transformation. For a low number of cycles, a higher peak is situated at a higher temperature, while for 3324 cycles, the opposite is true, indicating a change in the proportions of the two structures that is probably associated with the deformation mechanisms. This double peak could be interpreted as the inverse transformation of martensite to austenite with the transitory formation of phase R or another effect. To better understand the origin of this double transformation, supplementary DSC tests are necessary.

Immediately after heat treatment, for the untested material, a trace of R-phase was observed in the DSC thermogram (Fig. 3b). The heat flow peak for this phase in the untested material is very low compared with that of the same in the cycled material. This study highlights that the presence of the R-phase is due to cycling. Many studies show that the temperature of each transition phase (M_s, M_f, A_s and A_f) and the peak temperatures (M_p and A_p) are affected by heat treatment [10,17,19,25,26]. Similarly, cyclic loading is an important parameter that can disturb phase transformation temperatures and may give rise to the formation of the intermediate phase (R-phase).

3.3. Nanomechanical properties

For each sample, six series of 49 indentations were performed, and the mean values of the microhardness, the indentation modulus and creep capacity as well as the maximum depth under the load at the end of the creep time are given in the Table 2.

The standard deviation is lower than 2% for the microhardness, which is a rather good result for this material with respect to its microstructure. Regarding its variation during cycling, the microhardness increases by 5.2% between 1 cycle and 40 cycles, where it reaches a maximum and then slightly decreases by 2.2% between 40 cycles and failure at 3324 cycles.

The standard deviation of the indentation modulus is also below 2%. The modulus follows the same tendency observed for the microhardness, with variations of 3.5% between 1 cycle and 40 cycles and 5.8% between 40 cycles and failure.

For the creep behaviour, the standard deviation is in the range of 3.6%–4.3%. Compared to the microhardness and indentation modulus, the creep behaviour follows an inverse tendency, exhibiting first a decrease of 1.5% followed by an increase of 2.6%. This tendency appears reasonable.

As described in the previous paragraph, after the first unloading, no residual strain was observed, the material being completely in the austenitic phase. Irreversible strain started to appear at the end of the second unloading. Thus, , the material was not entirely in the austenitic phase; certainly, some residual martensite was present. From the 1st cycle to the 40th cycle, the structure of the material changed: a small part of the austenitic phase was transformed into residual martensite. This phase change implies a microstructural change [27] and may explain the evolution of mechanical properties such as the microhardness, indentation modulus and creep. The same type of observation has been reported by Delobelle et al. [28]. These authors demonstrated that the indentation modulus increases with grain size. They also observed that grain orientation has an important

Table 2
Mean values of microhardness, modulus, creep and maximum depth.

	HV (Kg/mm^2)	EIT (GPa)	CIT (%)	h_{max} (μm)
1 cycle	438 ± 6	91.8 ± 1.1	3.87 ± 0.15	0.534 ± 0.004
40 cycles	461 ± 7	95.0 ± 1.0	3.81 ± 0.14	0.520 ± 0.004
3324 cycles	450 ± 9	89.5 ± 1.5	3.91 ± 0.17	0.531 ± 0.005

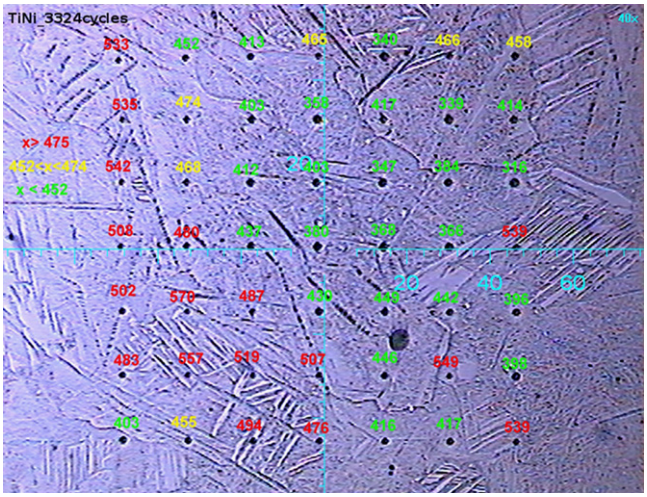

Fig. 4. Micrography of a series of indentations (squares measuring 200 μm × 200 μm) showing the distribution of hardness as a function of grain size.

Table 1
Temperatures (°C) of the different transformation stages.

	A_s	A_f	A_p	R_s	R_f	R_p	M_s	M_f	M_p
1 cycle	16.7	42.6	36.3	39.2	26.9	31.0	8.4	−31	−7.9
40 cycles	16.6	42.3	36.7	39.7	27.0	31.6	7.4	−34	−9.4
3324 cycles	15.1	44.1	23.5	41.3	23	28.4	-8	−39	−23.8
Untested Material	18	29.4	23.4	32.5	21.5	25.7	0	−23.4	−8.3

influence on nanomechanical properties. Fig. 4 shows that the indentation sizes (or the hardness values) are not randomly distributed but correspond to the microstructural characteristics of the specimens. To characterise the evolution of the microstructure during cycling in very fine detail, further analysis by low-cycle fatigue tests coupled with electron backscatter diffraction (EBSD) is necessary.

To examine the effect of fatigue loading on TiNi instruments, Jamlech et al. [29] used the nanoindentation technique. They compared fractured instruments with new ones. Their results highlighted the fact that the fatigue process revealed a significant decrease in the hardness and elastic modulus of the TiNi instruments. These authors concluded that the fatigue process did not result in work hardening but rather work softening. Indeed, from the 1 cycle to 3324 cycles (failure of the specimen), our results showed work softening as well. However, if the results of the 40th cycle are taken into account, this conclusion must be modified. The TiNi shape memory alloy undergoes work hardening during the first part of cycling, perhaps during the stabilisation of the CSS behaviour [9], which in this study corresponds to the first 40 cycles. Once the CSS behaviour is stabilised, there is no evolution in the shape of the hysteresis loops [12] and work softening can be observed.

3.4. TEM observations

Very few studies on TiNi memory shape alloys using low-cycle fatigue tests coupled with TEM observations have been reported in the literature [30,31]. To have a better understanding of the cyclic deformation mechanisms that occur in these materials, TEM observations were performed after each stopped low-cycle fatigue test.

After the first cycle, the deformation microstructure is characterised by a rather low dislocation density (Fig. 5), which suggests no real interaction between dislocations. A pile-up, however, is visible near the top edge of the grain. Very thin microtwins, approximately 2 nm to 3 nm in width, can also be seen locally (Fig. 6a and b). Almost everywhere, a high density of small precipitates can be seen, as in the uncycled material (Fig. 7). Their mean size ranges between 25 nm to 15 nm.

After 40 cycles, the dislocation density is slightly higher, but the microtwins are larger (between 50 nm and 100 nm) and more numerous (Fig. 8a and b). Furthermore, a new phenomenon occurs in which a three-part distribution in precipitate size is produced, the first one ranging between 25 and 18 nm (in the left part of Fig. 9), similar to that observed after 1 cycle, the second one ranging between 16 and 10 nm and the third one ranging between 6 and 2 nm (in the right part of Fig. 9). This occurs because the precipitates are shorn by mobile dislocations as shown in Fig. 10 (Fig. 10a–Fig. 10b). At this stage of cycling, not all of the precipitates have been shorn because dislocations are not very numerous and some areas keep the precipitates in the state they adopt in the uncycled material. In the areas where dislocations have shorn the precipitates, two distributions with precipitates cut once or twice and precipitates cut several times are observed, which likely reach the threshold of critical size before dissolution.

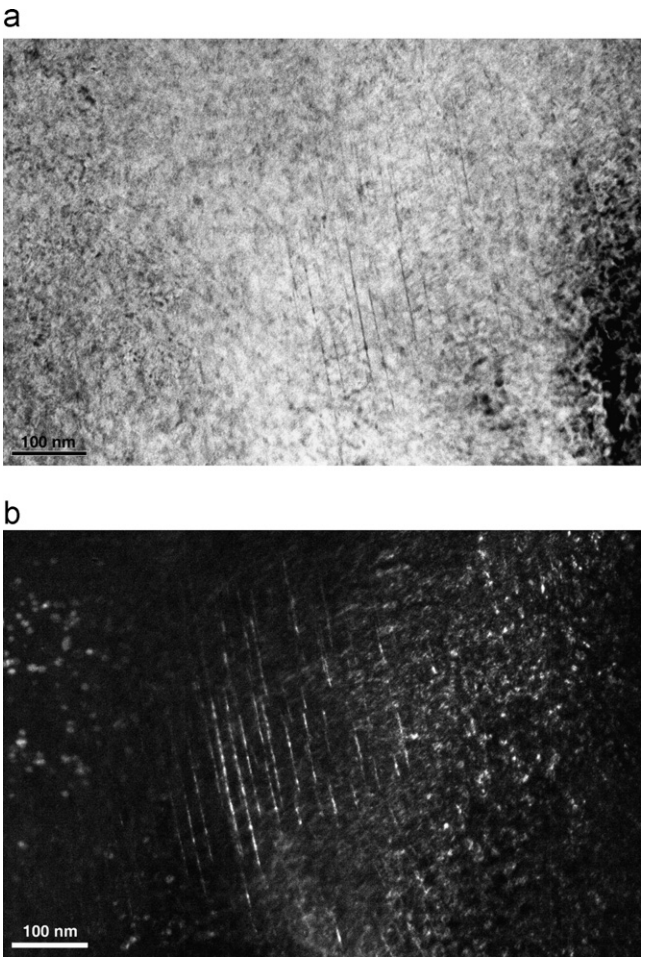

Fig. 6. Deformation microstructure after 1 cycle: thin microtwins (a–bright field; b–dark field).

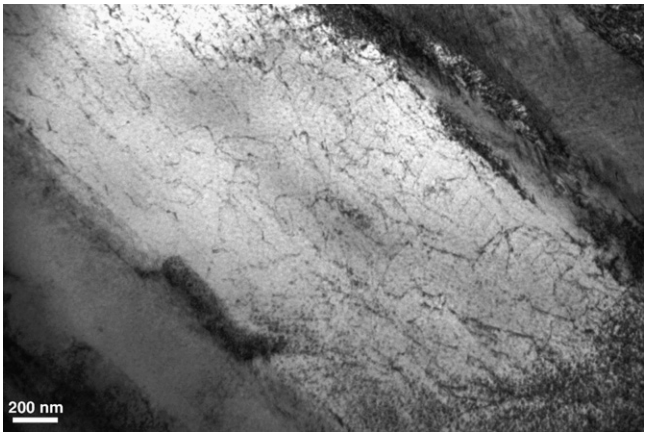

Fig. 5. Deformation microstructure after 1 cycle: low density of dislocations.

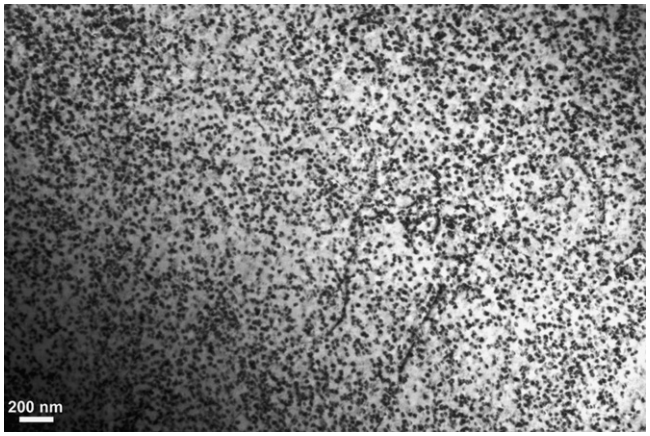

Fig. 7. High density of small precipitates in the uncycled material.

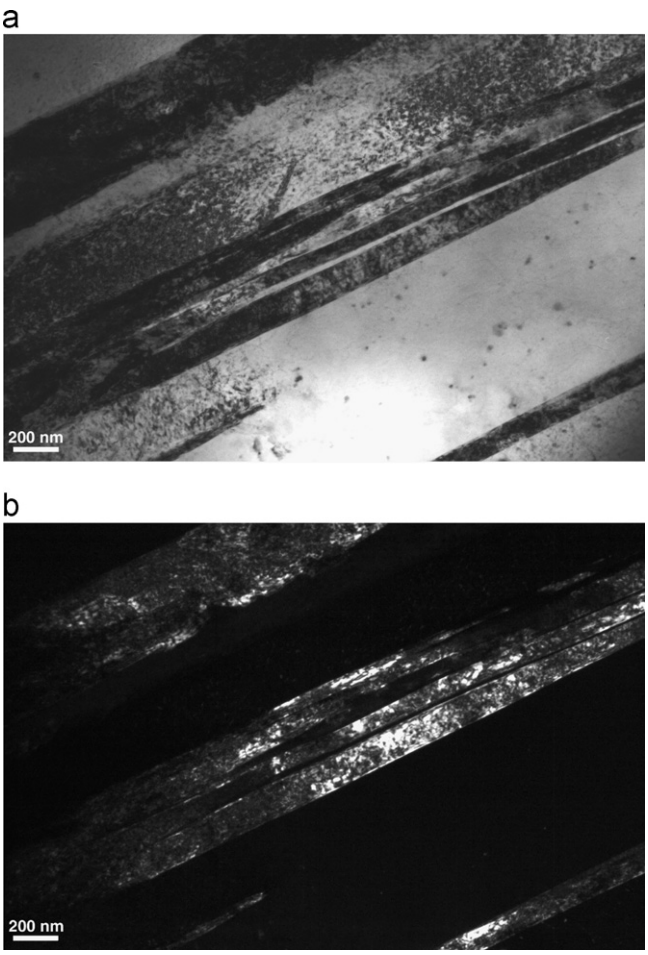

Fig. 8. Deformation microstructure after 40 cycles: growth of microtwins (a–bright field; b–dark field).

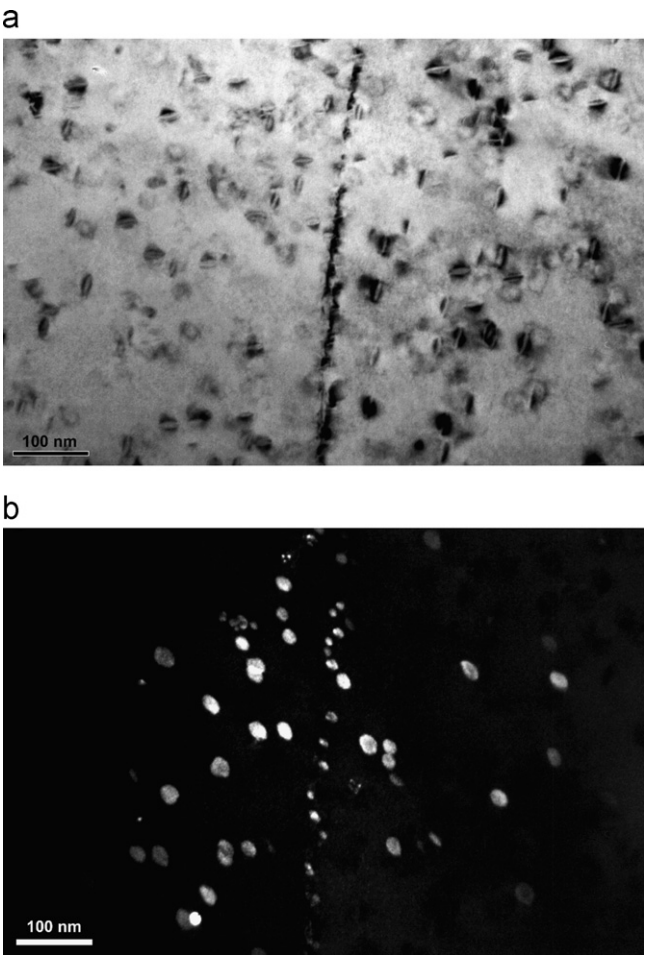

Fig. 10. Dislocation shear precipitates (a–bright field; b–dark field).

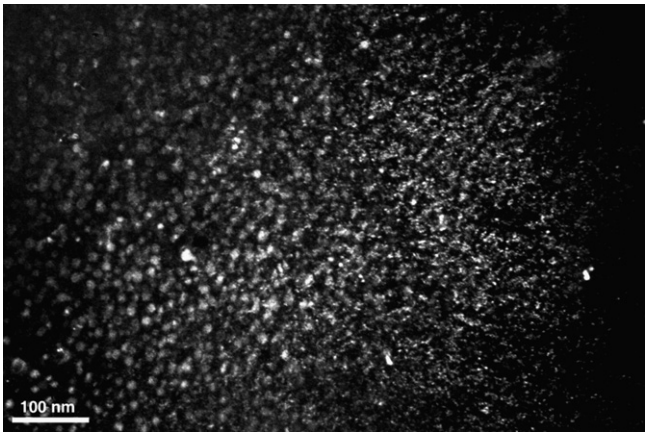

Fig. 9. Deformation microstructure after 40 cycles: three-part distribution in precipitate size.

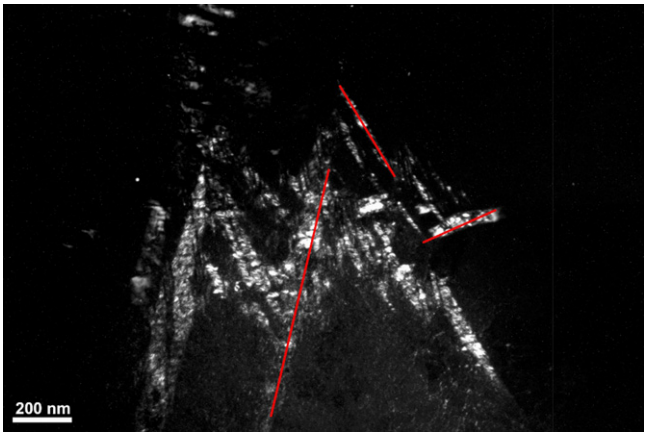

Fig. 11. Deformation microstructure after failure: high density of twins.

After failure, the dislocation density is higher than that at a low number of cycles but not very high. Moreover, the density of twins is higher, with sometimes two or even three systems in a grain (lines in Fig. 11), but not everywhere. At the same time, the precipitate distribution has evolved towards a non-homogeneous configuration with precipitate-free channels (Fig. 12). The localisation of the dislocation activity is probably responsible for the lack of precipitates in these channels due to the shearing of precipitates, as observed at 40 cycles. Indeed, the shearing of a precipitate by several dislocations will induce a decrease in the size of the precipitate and later its dissolution below its critical size. Locally, the presence of the R-phase was noted, as well as some small domains of martensite with a mean size of 200 to 300 nm.

From the first cycle to failure, there seem to exist two mechanisms of deformation that develop simultaneously without competition: microtwinning and the localisation of gliding dislocations that shear the precipitates and form channels free of them. The observations reported here are partly in agreement with those published in the literature. The presence of twinning

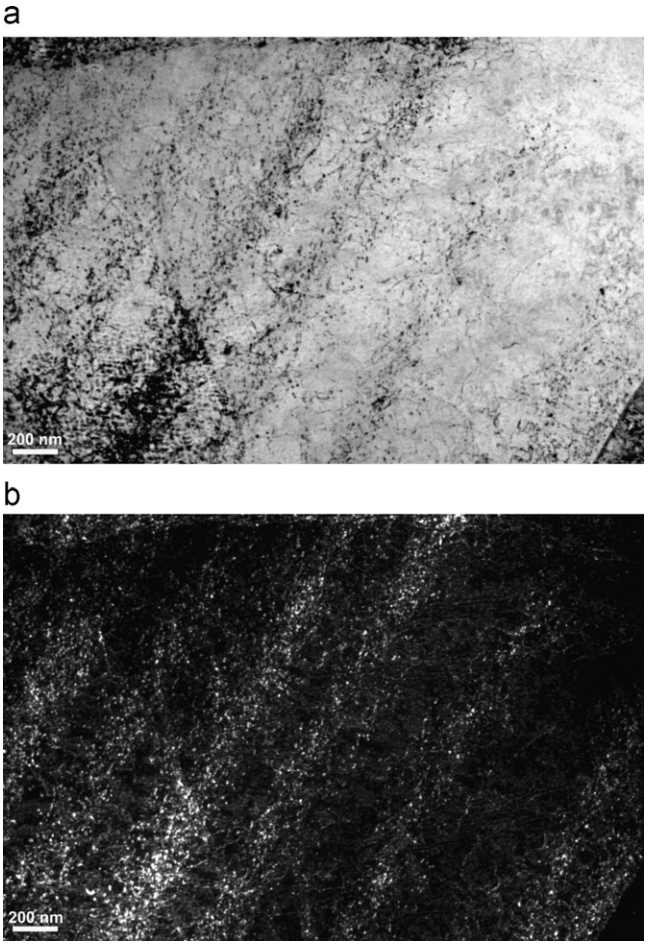

Fig. 12. Channels with free precipitates (a–bright field; b–dark field).

has already been described by Tan et al. [32] using a tensile test. The researchers reported observing the twinning phenomenon only along the stress plateau, during martensite transformation. Continuing deformation beyond the stress plateau induces detwinning of the martensite, accompanied by the production of dislocations [32]. In our study, we did not observe this detwinning. On the contrary, starting from the first cycle, very thin microtwins were observed locally, which continued to develop up to failure. Perhaps further investigations are necessary to clear this point. However, as observed by aforementioned authors, dislocations were indeed produced beyond the stress plateau. Compared with the uncycled material, the number of dislocations slightly increased from the first cycle. As reported in the work of Delville et al. [30], the dislocation density slightly increases during cycling. In this study, after 40 cycles, as observed after failure, dislocations shear precipitates. This result is in agreement with that reported by Michutta et al. [33]: precipitate size is directly governed by the density of dislocations. After failure, the precipitate distribution evolves towards a non-homogeneous configuration with precipitate-free channels. The disappearance of precipitates in the channels contributes to an increase in microtwinning to weaken nanomechanical properties such as the microhardness and the indentation modulus. Several authors [13,30,34] have reported that dislocations are created during the formation of martensite in TiNi. In this study, a rather low density is observed after the first cycle. Thus, are dislocations formed only from the austenite to martensite regime or in the reverse transformation as well? To answer this question, further investigations are necessary. Other authors [14,35] suggest that the irreversible strain results from residual martensite. During unloading, all of the martensite was not completely transformed into austenite. In this study, small domains of martensite were observed but only after failure. Therefore, no real relationship can be established between these domains and the presence of irreversible strain. Indeed, it is between the 1st and the 40th cycle that irreversible strain strongly increases. However, no martensite domain was observed after 40 cycles. For about the same number of cycles, 10 cycles, Delville et al. [30] also observed no residual martensite by TEM of the microstructure of cycled TiNi. They associated the presence of irreversible strain with an accumulation of dislocations. The observations reported here are more in line with this argument.

4. Conclusion

The aim of this study was twofold: first, to identify and to understand the deformation mechanisms that appear during the cyclic loading and particularly during the low-cycle fatigue of TiNi SMA and to explain how these deformation mechanisms can modify the nanomechanical properties of this material, such as the microhardness or indentation modulus.

The main results may be summarised as follows:

(1) It is clear that the cyclic stress-strain behaviour of TiNi SMA is composed of two stages. In the first stage, during the first 100 cycles, the hysteresis loops evolve, changing their form and becoming smaller, with emergence of irreversible strain at the end of the second unloading. At the same time, two deformation mechanisms expand simultaneously and without competition: twinning and gliding dislocations. During cyclic loading, twins become larger and dislocations glide easily and shear precipitates. These two mechanisms imply a slight increase in the hardness and indentation modulus but have no strong influence on the transformation temperatures. The appearance and the increase of irreversible strain in this stage are due to an accumulation of dislocations.

(2) In the second stage, a stabilisation of the cyclic strain-stress behaviour is observed without additional irreversible strain. Two mechanisms are always present: the density of twins and dislocations is slightly increased and the precipitate distribution evolves towards a non-homogeneous configuration due to precipitate shearing by dislocations. This mechanism induces a micro-structure constituted of walls containing a high density of small precipitates and separated by precipitate-free channels. The development of this structure involves an increase in twinning and, simultaneously, work softening, and a very marked shift in the transformation temperatures towards lower temperature are observed.

References

[1] C. Boller, In: M. Friswell (Eds.), Adaptative aerospace structures with smart technologies-a retrospective and future view adaptative structures: engineering applications, Inc. New-York, 2007, pp. 163–190.
[2] F.E. Feninat, G. Laroche, M. Fiset, D. Mantovani, Adv. Eng. Mater. 4 (2002) 91–104.
[3] K. Otsuka, X. Ren, Intermetallics 7 (1999) 511–528.
[4] P. Krulevitch, A.P. Lee, P.V. Ramsey, J.C. Trevino, J. Hamilton, M.A. Northrup, J. Microelectromech. Syst 5 (1996) 270–282.
[5] O. Doare, A. Sbarra, C. Touzé, M. Ould Moussa, Z. Moumni, Int. J. Solid. Struct 49 (2010) 32–42.
[6] S. Eucken, T. Duering, Acta Metal 37 (1989) 2245–2252.
[7] Z. Moumni, A. Vanherpen, P. Riberty, Smart Mater. Struct. 14 (2005) S287–S292.
[8] S. Nemat-Nasser, W. Guo, Mech. Mater. 38 (2006) 463–474.

[9] A. Paradis, P. Terriault, V. Brailovski, V. Torra, Smart Mater. Struct. 17 (2008) 1–11.
[10] Q. Liu, X. Ma, C. Lin, Y. Wu, Mater. Sci. Eng. A. 438-440 (2006) 563–566.
[11] M. Piedboeuf, R. Gauvin, J. Sound Vib. 214 (1998) 885–901.
[12] A.L. Gloanec, P. Cerracchio, B. Reynier, A. Vanherpen, P. Riberty, Scripta Mater. 62 (2010) 786–789.
[13] S. Miyazaki, T. Imai, Y. Igo, K. Otsuka, Metal. Trans. A-Phys. Metal. Mater. Sci 17 (1986) 115–120.
[14] C. Dunand-Châtellet, Z. Moumni, Int. J. Fatigue. 36 (2012) 163–170.
[15] J. Shaw, S. Kyriakides, J. Mech. Phys. Solids. 43 (1995) 1243–1281.
[16] Z. Wang, X. Zu, X. Feng, H. Mo, J. Zhou, Mater. Lett. 58 (2004) 3141–3144.
[17] P. Filip, K. Mazanec, Scripta Metal. Mater 32 (1995) 1375–1380.
[18] A. Paula, J. Canejo, N. Schell, F. Braz Fernades, Nucl. Inst. Meth. Phys. Res. B 238 (2005) 111–114.
[19] H. Shahmir, M. Nili-Ahmadabadi, F. Naghdi, Mater. Des 32 (2011) 365–370.
[20] A. Miller, D. Lagoudas, Mater. Sci. Eng. A. 308 (2001) 161–175.
[21] D. Chroback, D. Stroz, Scripta Mater. 52 (2005) 757–760.
[22] Y. Zhou, G. Fan, Mater. Sci. Eng. A. 438-440 (2006) 602–607.
[23] J. Kim, K. Liu, S. Miyazaki, Acta Mater. 52 (2004) 487–499.
[24] J. Uchil, F. Braz Fernades, K. Malesh, Mater. Charact. 58 (2007) 243–248.
[25] J. Marquez, T. Slater, F. Sczerzenie. Determining the transformation temperatures of TiNi alloys using differential scanning calorimetry. In *Proceedings of the Second International Conference on Shape Memory and Superelastic Technologies (SMST-97)*. 1997.
[26] Y. Wang, Y. Zheng, Y. Liu, J. Alloys Compd 477 (2009) 764–767.
[27] J.A. Shaw, C.B. Churchill, M.A. Ladicola, Exp. Tech. 32 (2008) 55–62.
[28] P. Delobelle, S. Dali, F. Richard, Mater. Tech 99 (2011) 185–196.
[29] A. Jamlech, A. Sadr, N. Nomura, Int. Endodontic J. 45 (2012) 462–468.
[30] R. Delville, B. Malard, J. Pilch, P. Sittner, D. Schryvers, Int. J. Plasticity. 27 (2011) 282–297.
[31] S. Kajiwara, Metal. Trans. A 17 (1986) 1693–1702.
[32] G. Tan, L. Yinong, P. Sittner, M. Saunders, Scripta Mater. 50 (2004) 193–198.
[33] J. Michutta, M. Carroll, A. Yawny, C. Somsen, K. Neuking, G. Eggeler, Mater. Sci. Eng. A. 378 (2004) 152–156.
[34] T. Simon, A. Kröger, C. Somsen, A. Dlouhy, G. Eggler, Acta Mater. 58 (2010) 1850–1860.
[35] K. Gall, H.J. Maier, Acta Mater. 50 (2002) 4643–4657.